

An Investigation Into Thermal Performance of Buildings Built Using Upcycled End-Of-Life Photovoltaic Panels

Roshan R Rao – Indian Institute of Science, India – roshanrao@iisc.ac.in

Suchi Priyadarshani – Indian Institute of Science, India – suchip@iisc.ac.in

Monto Mani – Indian Institute of Science, India – monto@iisc.ac.in

Abstract

End-of-Life, or discarded, Solar Photovoltaic panels are rising in huge numbers every year throughout the world. This is of grave concern as the environmentally safe handling of EoL-PV is not yet established fully. We propose a novel approach to upcycle End-of-Life (EoL)-PV as a building material that can extend the life of PV by another 2-3 decades. PV panels are a multi-layered laminate of different materials. In the course of environmental exposure and use, degradation induces variation in the optical properties of EoL-PV. Variations in thermal properties have not been explicitly examined, which has a bearing on the thermal performance of a building when integrated as a building material. This work studies the influence of the thermal conductivity and solar transmittance of PV panels on the surface temperatures using a steady-state energy balance model. Also, through the whole building simulation, the implications on the mean radiant temperature and the heating/cooling load of the building by using EoL PV compared to a new PV are understood. Other factors, like the area of PV to wall ratio, seasonal changes, and climate zone are found to play a role in the relative changes in the MRT and Heating/Cooling Load attributed to EoL-PV integration in buildings.

1. Introduction

Solar Photovoltaic (PV) installations are growing exponentially worldwide, leaving behind a massive pile of PV waste after its decommissioning. By 2050, cumulative PV waste would be 60-78 million tons (IEA-PVPS and IRENA, 2016). Currently, most PV panels end up in shredders and/or landfills, contaminating and disrupting our ecosystem. We propose a novel approach to upcycle End-of-Life (EoL)-PV as a building material that can extend the life of PV by another 2-3 decades. On another note, the num-

ber of people living in slums or informal settlements is over 1 billion, with 80 % in Eastern and South-Eastern Asia, sub-Saharan Africa and Central and Southern Asia. About 3 billion people will require adequate and affordable housing by 2030 (United Nations, 2021).

EoL-PV panels are a low-cost alternate durable option as a building material, and this approach promotes planetary wellness by offsetting the use of conventional materials and preventing toxic elements in PV entering the ecosystem. On using PV panels as a building façade, the occupants are exposed to the backsheet of the PV panel. Backsheet chalking (presence of white coloured powder on the backsheet) is commonly observed in field degraded PV. In a few cases, it has been investigated and discovered to be TiO_2 (Gebhardt et al., 2018), and usage of such PV panels in buildings exposes the occupants to such powders. Also, the release of fluorine from the backsheet has been examined at high temperatures ($> 300\text{ }^\circ\text{C}$) (Danz et al., 2019). The release of fluorine at room temperature or the nature of the impact of chalking on occupants has not been understood. Studies involving any emissions from PV backsheet (due to cracking, chalking, burns, etc.) and its negative impact on occupants is essential.

PV panels are laminate of different materials. A typical PV panel configuration is Glass / EVA / Cell / EVA / Backsheet and layers of anti-reflective coating subject to the manufacturer. A commonly observed degradation mode in PV is EVA (ethylene vinyl acetate) discoloration, which occurs due to acetic acid formation (Pern & Czanderna, 1992). Also, the adhesion strength of the EVA (primarily used as an adhesive layer in panels) is compromised in aged PV (Desai et al., 2022), which could lead to delamination of PV panels. A change in vinyl acetate (VA)

content has been reported in the aged PV panel (Desai et al., 2022). VA content change can imply a change in the thermal conductivity of the EVA (Jia and Zhang, 2022) layer in the PV panel. Also, due to discoloration of the EVA layer, optical transmittance is reported to have dropped (Desai et al., 2020; Jeong et al., 2013). Due to the inherent nature of PV panels being composed of multiple layers of different materials, unlike a homogenous panel, physical and chemical changes in any layer impact the optical and thermal properties of the bulk material. Our preliminary investigations include understanding the influence of physical degradation on optical and thermal transmittance of EoL-PV (aged) and its influence on the building's thermal performance and indoor thermal comfort. A steady-state energy balance model is used to understand the effect of changes in optical and thermal properties on PV surface temperatures. When PV panels are integrated as a building elements, multiple other factors influence the thermal performance of the building. Hence, a whole building simulation is performed using Design Builder software with EoL-PV integrated with the building.

2. Methodology

2.1 Energy Balance Model

An optical model considering the interaction of light through multiple layers of PV is used to calculate the spectral transmittance, reflectance and absorptance of the PV panel at each layer (Lu & Yao, 2007). The heat transfer modes among the layers considered are shown in Fig. 1. The transmittance, reflectance, and absorptivity of n (number of layers) layers of the PV panel are calculated using the multi-layered optical model developed (Lu & Yao, 2007).

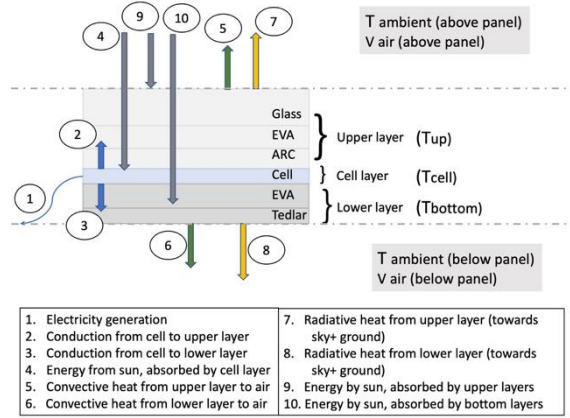


Fig. 1 - Heat transfer modes at different layers of a typical PV module

A steady-state energy balance model for PV panel is used, which considers the heat transfer through multiple layers of PV panel (Glass, EVA, ARC, Si-cell, EVA, Tedlar). The angle between the sun and the normal to PV panel is calculated using the following equations

$$a = (\sin \phi \cdot \sin \delta \cdot \cos \beta) - (\cos \phi \cdot \sin \delta \cdot \cos \gamma_m \cdot \sin \beta) \quad (1)$$

$$b = (\sin \phi \cdot \cos \delta \cdot \cos \gamma_m \cdot \sin \beta) + (\cos \phi \cdot \cos \delta \cdot \cos \beta) \quad (2)$$

$$c = (\cos \delta \cdot \sin \gamma_m \cdot \sin \beta) \quad (3)$$

$$\theta = \cos(a + b \cos \omega + c \sin \omega) \quad (4)$$

Electricity generated depends on the net radiation transmitted through the first three layers and the efficiency of the solar cell (Zarei & Abdolzadeh, 2016). The rate of energy absorption by a Solar cell depends on the absorptivity of the cell layer.

$$q_4 = \int_0^{\infty} A_{cell}(\lambda) \cdot g(\lambda) d\lambda \quad (5)$$

$$q_1 = \eta_{electricity} \int_0^{\infty} \tau_u(\lambda) \cdot g(\lambda) d\lambda \quad (6)$$

Bi-directional (towards the upper and lower layers) conduction from the cell depends on the temperature differences and the thermal conductivity of the corresponding layers (Zarei & Abdolzadeh, 2016).

$$q_{2,3} = \frac{T_{cell} - T_{u,b}}{R_{u,b}} \quad (7)$$

Convective heat transfer occurs at the top layers-air interface, and the bottom layers-air interface is a function of the temperature difference and heat transfer co-efficient. The heat transfer coefficient approximations are adapted from (Zarei & Abdolzadeh, 2016).

$$q_{5,6} = h_{u,b} \cdot (T_{u,b} - T_{air-film\ u,b}) \quad (8)$$

Radiative heat transfer between the top layers-sky, top layers-ground and bottom layers-sky, bottom layers-ground is a function of view factor and temperature difference (Zarei & Abdolzadeh, 2016).

$$q_7 = \varepsilon_u \sigma F_{u,sky,ground} (T_u^4 - T_{sky,ground}^4) \quad (9)$$

$$q_8 = \varepsilon_b \sigma F_{b,sky,ground} (T_b^4 - T_{sky,ground}^4) \quad (10)$$

$$q_{9,10} = \int_0^\infty A_{u,b}(\lambda, \theta) \cdot g(\lambda) d\lambda \quad (11)$$

The above system of equations was solved for top, bottom, and cell temperatures through an iterative approach. The thickness of Glass, EVA, Cell and Backsheet is in the range of 3-4 mm, 0.4-0.5 mm, 0.2-0.4 mm, and 0.1-0.35 mm, respectively.

The thermal conductivity of Glass, EVA, Cell and Backsheet are in the range of 0.98 – 1.8 W/(m K), 0.23-0.35 W/(m K), 148-150 W/(m K), and 0.2-0.36 W/(m K), respectively (Chamkha & Selimefendgil, 2018; Hammami et al., 2017; Lee et al., 2008; Popovici et al., 2016; Sahli et al., 2018; Syafiqah et al., 2019). The thickness and thermal conductivity used as a base case in the steady-state model: glass (3 mm, 0.98 W/(m K)), EVA (0.5 mm, 0.35 W/(m K)), cell (0.4 mm, 148 W/(m K)), back sheet (0.1 mm, 0.2 W/(m K)).

To understand the influence of the thermal conductivity of each layer on the surface temperatures, thermal conductivity values were varied from -100 % ~ +200 % of the base-case values.

2.2 Design Builder Model

A whole building simulation has been performed for the modified BESTEST case 600FF (Design-Builder v6.1 with EnergyPlus v 8.9, 2021) model (a block of 6 m X 8 m and height of 2.7 m) (Fig. 2). PV panels have been integrated in the buildings as Glazing integrated Photovoltaics. PV panels are applied to substitute for the walls and roof and not over the existing wall or roof. The properties of the PV (250 Wp typical crystalline Silicon PV panel): (a) front and back emissivity is 0.8, infrared transmittance is 0.2, inside and outside reflectance (solar and visible) is 0.1, and the thermal conductivity, solar transmittance is varied in the range tabulate in Table 1. The PV panels are not connected to any power

sources in the simulation and are only considered a building material. Simulations are performed for varying PV area in the wall (varied as window-to-wall ratio in the Design Builder) for two cases, 25 % and 75 %. Multiple scenarios of PV integration in all four walls and roof are considered. The wall (without PV) is the 'BESTEST Lightweight Wall', which has a concrete cast (dense) with a thickness of 0.1m (see Fig. 2). The floor construction is 'BESTEST Ground Floor', which has a thickness of 0.225 m and a U value of 0.039 W/(m² K). The roof (without PV) is 'BESTEST Roof' with a U value of 0.319 W/(m² K) and thickness of 0.1 m. The simulation is performed with an occupancy density of 0.04 people/m² and no furniture/furnishings in the building. The BESTEST building being simulated is a block with a heating and cooling setpoint temperatures of 20 °C and 26 °C, respectively. India has varied climate zones, and simulations are performed for five representative cities corresponding to five climate zones (Table 2).

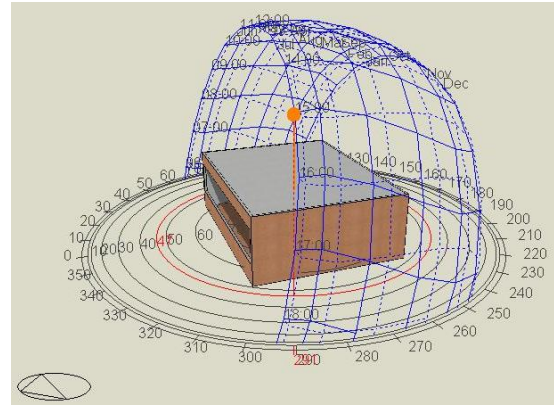


Fig. 2 – Design Builder model (600FF) modified by integrating PV in all the walls and roof

The thermal conductivity of the EVA layer varies due to the variation in the % VA content. An empirical relation has been proposed (Jia et al., 2022) to describe the relationship between thermal conductivity and % VA content.

With ageing, a maximum change in VA content in EVA was seen, with an increase from 18.1 % to 21.9 % (Desai et al., 2022). This is estimated to cause a drop in thermal conductivity of EVA and the bulk of PV panels. But this does not explain any changes in the bulk thermal conductivity. There are possibilities of reduction in the thickness (Hu et al., 2016; Jahn, 2018) of the back sheet due to weathering, and

this can cause the bulk thermal conductivity to rise. Hence, there is a possibility that the bulk thermal conductivity may get altered depending on the combination and severity of multiple degradation modes. To accurately quantify the change in thickness, thermal conductivity of the individual layers and bulk properties associated with aged PV panels (EoL-PV) requires sophisticated measurements. To broadly understand the impact of such a change at the building level, we have varied the bulk thermal conductivity (equivalent thermal conductivity of a PV panel including all the layers) and solar transmittance of the PV panels in 5 steps each. A total of 25 scenario combinations of PV panel have been considered for whole building simulations (Table 1).

Table 1 – Range of Thermal conductivity and Solar Transmittance values. Corresponding SHGC and U-value of all the possible combinations

Parameter	Range	Steps
Thermal Conductivity	0.1 ~ 2.8 W/(m K)	0.7 W/(m K)
Solar Transmittance	0.1 % ~ 16 %	4 %
SHGC (calculated)	0.271 ~ 0.408	-
U- Value (calculated)	4.763 ~ 5.782 W/(m ² K)	-

Table 2 – The representative cities selected for each climate zone in India

Climate Zone	City	Lat/Long (°North / °East)	Mean Daily Temp (°C) (min ~ max)
Temperate	Bangalore	12.97 / 77.58	15.0 ~ 33.9
Composite	Lucknow	26.75 / 80.88	7.3 ~ 40.3
Warm-Humid	Kolkata	22.65 / 88.45	13.7 ~ 35.7
Hot-Dry	Ahmedabad	23.07 / 72.63	13.1 ~ 41.4
Cold	Shillong	25.58 / 91.89	4.4 ~ 24.0

To allow for a comparative assessment between an EoL PV panel and a new panel, the new panel has been considered to have a thermal conductivity of 0.7 W/(m K) and 8 % solar transmission. Mean

Radiant Temperature (used as a heat index to indicate thermal comfort) and Heating/Cooling loads resulting from 25 combinations of PV panels have been analyzed. Simulations are performed to understand the influence of PV covered area to wall area ratio, the direction of the envelope on which the PV panels are integrated and Climate zone.

3. Results and Discussion

When the thermal conductivity of the glass layer is varied from -100 % to 200 % of its reference value (0.9 W/(m K)), the top layer's thermal resistance increases exponentially with the decrease in the thermal conductivity of glass. The increase in the thermal resistance in the top layer causes a drop in the rate of conduction heat transfer between cell and top layer. This causes a reduction in the top layer energy, as the radiation absorption by the top layer is unaffected by the change in the thermal conductivity of the glass. The decrease in the top layer energy is associated with the reduction in the top layer temperature. As the energy balance between energy into the cell and out of the cell has to be maintained at the steady-state, the conduction heat transfer between cell-bottom layer increases. This causes the bottom layer energy to increase and results in the rise in temperature of the bottom layer (Fig. 3). Each layer's thermal conductivity variation impacts the PV panel's bulk thermal conductivity (equivalent thermal conductivity). The PV panel's bulk thermal conductivity (equivalent thermal conductivity) was varied to understand the bottom surface temperature variation, as this is the surface that will interact with the indoor air when integrated in the building. A surface temperature calculation is made for the scenario where the PV panel is horizontal, and solar radiation of 900 W/m² is incident on the PV panel (Fig. 4). Further, in the whole building simulation, the degradation of PV was parameterized as a variation in solar transmittance (τ) and thermal conductivity (k) (equivalent thermal conductivity) of PV. The different scenarios of PV are compared with the base case of PV, and only relative changes in MRT and Heating Cooling load with respect to the base case is reported throughout.

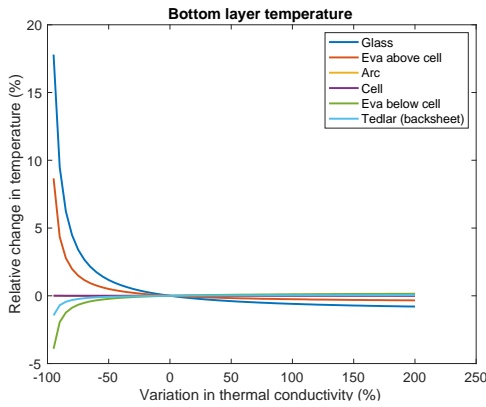


Fig. 3 – Bottom surface temperature variation with variation in the thermal conductivity of each layer of PV module

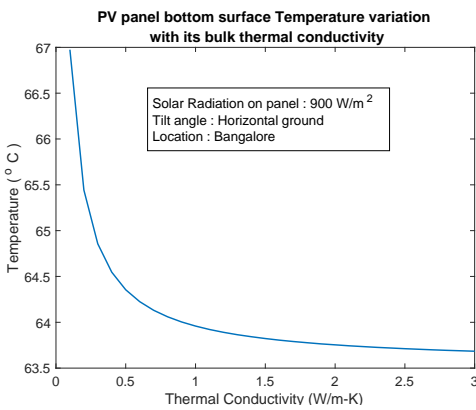


Fig. 4 – PV bottom surface temperature variation with the bulk thermal conductivity of PV panel (equivalent thermal conductivity of PV panel)

PV was integrated in the roof, and a typical summer week simulation revealed that, as the solar transmittance drops, there is about 2 % and 15 % drop in the relative change in Mean Radiant Temperature (MRT) and Heating Cooling load, respectively (Fig. 5). We understand from the literature that there are higher chances of solar transmittance drop due to EVA degradation, glass degradation, etc. The maximum and minimum relative changes in MRT and Heating Cooling load occur at maximum and minimum solar transmittance conditions. A typical summer week and winter week are compared for the maximum and minimum relative changes. Fig. 6 shows that the ranges of relative changes are broadened during winter, indicating that the external temperature has a role in indoor and MRT changes.

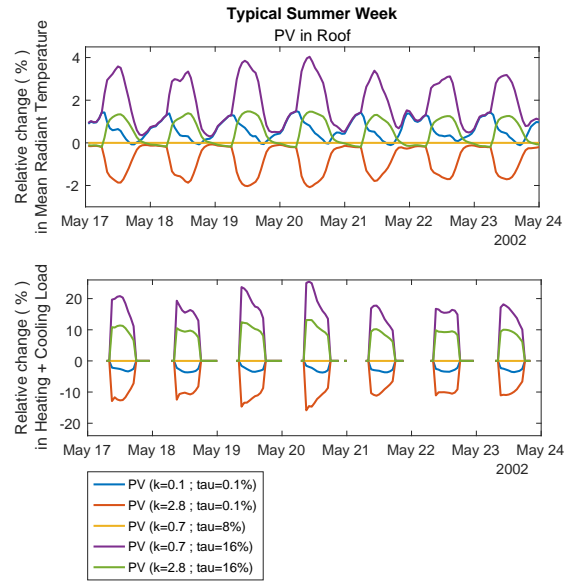


Fig. 5 – Relative change (%) in the Mean Radiant Temperature and Heating+Cooling Load for a typical summer week in Bangalore

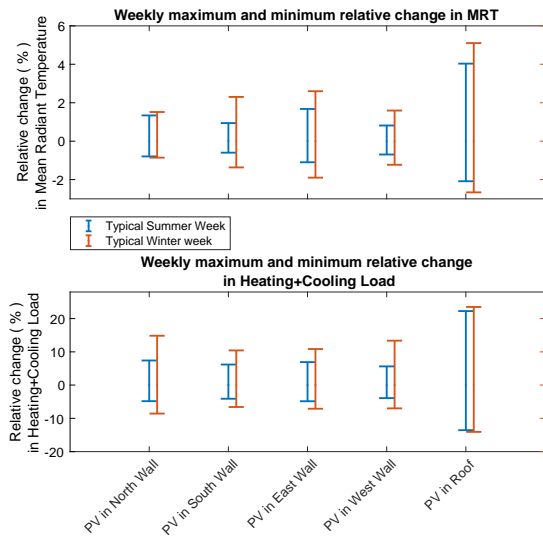


Fig. 6 – Weekly maximum and minimum relative change in MRT and Heating+Cooling Load when PV is integrated in North wall, South wall, East wall, West wall and Roof

The relative changes in MRT and Heating Cooling load variation with thermal conductivity of PV are investigated with a simulation of PV in the roof for a summer month (Fig. 7). The trend is similar to the trend observed using the steady-state energy balance model at the PV panel level (Fig. 4). The area ratio of PV to the wall also magnifies the range of minimum and maximum relative changes in the MRT and Heating Cooling load (Fig. 8).

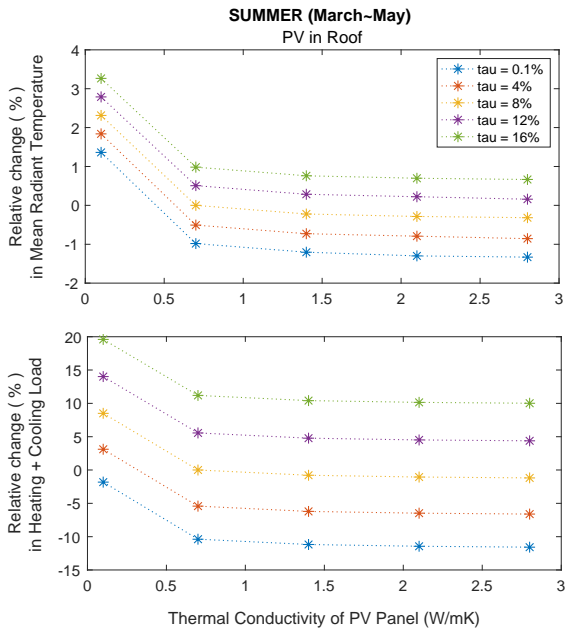


Fig. 7 – Influence of Solar Transmittance and Thermal Conductivity on the Relative change in MRT and Heating+Cooling Load

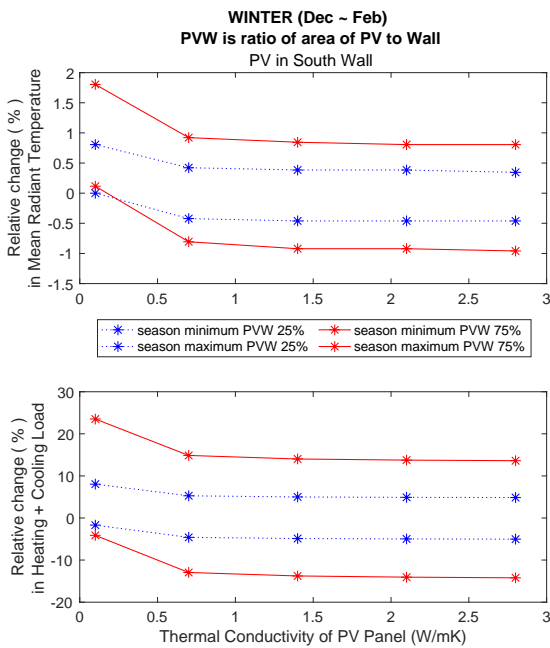


Fig. 8 – Influence of ratio of PV area-to-wall area on minimum and maximum relative changes in annual mean MRT and heating/cooling load

Annual mean MRT and Heating Cooling loads are calculated based on simulations run for all the days of the year. Such a simulation was performed to compare the relative changes in different climate zones and the location of application of PV in a building.

Annual Minimum relative change (%) in MRT					
Bangalore	-0.3824	-0.5977	-0.5568	-0.5241	-1.453
Ahmedabad	-0.2911	-0.5626	-0.5306	-0.4654	-1.388
Lucknow	-0.346	-0.6282	-0.522	-0.5281	-1.44
Kolkata	-0.2579	-0.5005	-0.3276	-0.4323	-1.112
Shillong	-0.823	-0.3065	-0.8039	-1.087	-1.963
	North	South	East	West	Roof
Annual Maximum relative change (%) in MRT					
Bangalore	0.9178	1.121	0.928	0.9734	3.702
Ahmedabad	0.5459	0.8439	0.7075	0.6445	3.311
Lucknow	0.7305	1.109	0.8949	0.8299	3.567
Kolkata	0.5158	0.7508	0.5461	0.6844	2.813
Shillong	1.875	0.6567	1.697	1.914	5.207
	North	South	East	West	Roof

Fig. 9 – Minimum and Maximum relative changes in annual mean MRT for different cities and PV application location in building

Fig. 9 and Fig. 10 tabulate the relative changes in the annual mean MRT and Heating Cooling load for different cities and the location in the building where PV is applied. The application of EoL PV on the roof seems to be more beneficiary in terms of reduction in MRT and Heating Cooling load. This could be possible due to the larger area exposed to the sun for longer hours than the walls.

4. Conclusion

This work has discussed a novel approach to up-cycle EoL PV panels into building applications. The bottom surface temperature of PV rises when the thermal conductivity of the PV panel reduces. Specifically, glass layer’s thermal conductivity variation has a dominant impact on temperature variation due to its thickness. Furthermore, whole building simulations also confirm the exponential temperature variation of mean radiant temperature with thermal conductivity. Our simulation indicates a drop of about 2 % in MRT and close to 13 % in Heating Cooling load due to the loss in solar transmittance and thermal conductivity of PV. The reduction of solar transmittance due to EVA degradation is widely reported in the literature, making it favorable for EoL PV in building applications. The application of EoL PV on the roof seems to be more beneficiary in terms of reduction in MRT and Heating Cooling load.

Annual Minimum relative change (%) in Heating+Cooling Load					
Bangalore	-4.822	-5.822	-5.513	-5.548	-12.74
Ahmedabad	-2.421	-4.049	-3.715	-3.549	-10.72
Lucknow	-2.556	-4.552	-3.955	-3.636	-10.49
Kolkata	-2.285	-3.614	-2.678	-3.492	-9.435
Shillong	-3.985	-6.761	-4.157	-6.04	-9.586
	North	South	East	West	Roof

Annual Maximum relative change (%) in Heating+Cooling Load					
Bangalore	8.45	9.813	8.929	8.675	22.02
Ahmedabad	2.999	5.694	5.116	4.625	18.27
Lucknow	3.181	6.675	5.514	4.862	17.68
Kolkata	3.166	5.135	3.683	4.65	15.83
Shillong	3.856	11.32	5.961	9.765	14.91
	North	South	East	West	Roof
	PV location				

Fig. 10 – Minimum and Maximum relative changes in annual mean Heating Cooling load for different cities and PV application location in building

The benefit is achieved in the case of lower solar transmittance conditions, which also implies lesser daylight entry into the building. The implication of this on the marginal rise in electricity consumption for artificial lighting is the scope of further study. There is no significant difference in the magnitude of relative changes in MRT or Heating Cooling loads at different climate zones. At this point, it can be argued that application of EoL PV has the potential to be used as a building material in general and provide better thermal performance at the same time. A more detailed understanding of the variations of optical and thermal properties due to different degradation modes permits us to speculate on the possible implication of EoL-PV applications in buildings more accurately.

Nomenclature

Symbols

$A_{cell,u,b}$	Absorptivity (cell, upper or bottom layers)
$F_{b,sky,ground}$	View Factor (bottom layer - sky or bottom layer - ground)
$F_{u,sky,ground}$	View Factor (upper layer - sky or upper layer - ground)
$h_{u,b}$	Convective heat transfer coefficient (W/m ² K) (upper or bottom layers)
$R_{u,b}$	Resistance in conduction (K/W) (upper or bottom layer)

$T_{air-film\ u,b}$	Temperature (°C) (air film upper or bottom layers)
$T_{cell,u,b}$	Temperature (°C) (cell, upper or bottom layer)
$T_{sky,ground}$	Temperature (°C) (sky or ground)
$\eta_{electricity}$	PV conversion efficiency
$\tau_{u,b}$	Transmittivity (upper or bottom layers)
ϕ	Latitude
g	Solar radiation (W/m ²) incident on PV panel
τ	Solar Transmittance
β	Tilt angle (degrees from horizontal)
δ	Declination angle (degrees)
θ	Inclination angle (degrees) between sun and normal to PV panel
ω	Hour angle (degrees)

References

- Chamkha, A. J. and F. Selimefendigil. 2018. "Numerical Analysis for Thermal Performance of a Photovoltaic Thermal Solar Collector with SiO₂-Water Nanofluid". *Applied Sciences* 8(11). doi: <https://doi.org/10.3390/app8112223>
- Danz, P., V. Aryan, E. Möhle, and N. Nowara. 2019. "Experimental Study on Fluorine Release from Photovoltaic Backsheet Materials Containing PVF and PVDF during Pyrolysis and Incineration in a Technical Lab-Scale Reactor at Various Temperatures". *Toxics* 7(47).
- Desai, U., B. K. Sharma, A. Singh, and A. Singh. 2020. "Enhancement of Resistance against Damp Heat Aging through Compositional Change in PV Encapsulant Poly (Ethylene-Co-Vinyl Acetate)". *Solar Energy* 211: 674–82. doi: <https://doi.org/10.1016/j.solener.2020.09.083>
- Desai, U., B. Kumar Sharma, A. Singh, and A. Singh. 2022. "A Comparison of Evolution of Adhesion Mechanisms and Strength Post Damp-Heat Aging for a Range of VA Content in EVA Encapsulant with Photovoltaic Backsheet". *Solar Energy* 231: 908–20. doi: <https://doi.org/10.1016/j.solener.2021.12.031>
- DesignBuilder v6.1 with EnergyPlus v 8.9, ANSI/ASHRAE Standard 140-2017 Building

- Thermal Envelope and Fabric Load Tests - Validation Report, 2021.
- Gebhardt, P., L. P. Bauermann, and D. Philipp. 2018. "Backsheet Chalking - Theoretical Background and Relation to Backsheet Cracking and Insulation Failures". In *35th European PV Solar Energy Conference and Exhibition*.
- Hammami, M., S. Torretti, F. Grimaccia, and G. Grandi. 2017. "Thermal and Performance Analysis of a Photovoltaic Module with an Integrated Energy Storage System". *Applied Sciences* 7(11). doi: <https://doi.org/10.3390/app7111107>
- Hu, H., W. M. Wang, O. Fu, A. Bradley, T. Felder, W. Gambogi, and T. J. Trout. 2016. "Typical Photovoltaic Backsheet Failure Mode Analysis under Different Climates in China". *SNEC International Photovoltaic Power Generation Conference*.
- IEA-PVPS and IRENA. 2016. *End-of-Life Management: Solar Photovoltaic Panels*.
- Jahn, U. 2018. *Methoden Zur Fehlererkennung Bei PV-Modulen Und Anlagen-Qualitaetsicherung Im Feld*, pp. 1–22.
- Jeong, J. S., and N. Park. 2013. "Field Discoloration Analysis and UV/Temperature Accelerated Degradation Test of EVA for PV". *2013 IEEE 39th Photovoltaic Specialists Conference (PVSC)*.
- Jia, Y. and J. Zhang. 2020. "Thermal Conductivity of Ethylene-Vinyl Acetate Copolymers with Different Vinyl Acetate Contents Dependent on Temperature and Crystallinity". *Thermochimica Acta* 708:179141. doi: <https://doi.org/10.1016/j.tca.2021.179141>
- Lee, B., J. Z. Liu, B. Sun, C. Y. Shen, and G. C. Dai. 2008. "Thermally Conductive and Electrically Insulating EVA Composite Encapsulant for Solar Photovoltaic (PV) Cell". *Express Polymer Letters* 2(5): 357–63. doi: <https://doi.org/10.3144/expresspolymlett.2008.42>
- Lu, Z. H., and Q. Yao. 2007. "Energy Analysis of Silicon Solar Cell Modules Based on an Optical Model for Arbitrary Layers". *Solar Energy* 81: 636–47, 2007. doi: <https://doi.org/10.1016/j.solener.2006.08.014>
- Pern, F. J., and A. W. Czanderna. 1992. "Characterization of Ethylene Vinyl Acetate (EVA) Encapsulant: Effects of Thermal Processing and Weathering Degradation on Its Discoloration". *Solar Energy Materials and Solar Cells* 25(1–2): 3–23, 1992. doi: [https://doi.org/10.1016/0927-0248\(92\)90013-F](https://doi.org/10.1016/0927-0248(92)90013-F)
- Popovici, C. G., S. V. Hudişteanu, T. D. Mateescu, and N. C. Cherecheş. 2016. "Efficiency Improvement of Photovoltaic Panels by Using Air Cooled Heat Sinks". *Energy Procedia* 85: 425–32. doi: <https://doi.org/10.1016/j.egypro.2015.12.223>
- Sahli, M., J. P. de Magalhaes Correia, S. Ahzi, and S. Touchal. 2018. "Thermomechanical Investigation of PV Panels Behaviour under NOCT Conditions". *Proceedings of 2017 International Renewable and Sustainable Energy Conference, IRSEC 2017*. doi: <https://doi.org/10.1109/IRSEC.2017.8477292>
- Syafiqah, Z., N. Amin, M. Irwanto, W. Z. Leow, and A. R. Amelia. 2019. "Thermal and Electrical Study for PV Panel with Cooling System". *Indonesian Journal of Electrical Engineering and Computer Science* 17(2): 941–49, 2019. doi: <http://doi.org/10.11591/ijeecs.v7.i2.pp492-499>
- United Nations. 2021. *Make Cities and Human Settlements Inclusive, Safe, Resilient and Sustainable*.
- Zarei, T., and M. Abdolzadeh. 2016. "Optical and Thermal Simulations of Photovoltaic Modules with and Without Sun Tracking System". *Journal of Solar Energy Engineering* 138(1): 1–12. doi: <https://doi.org/10.1115/1.4031684>